Maintenance of Multiple Jets in a Baroclinic Flow

SUKYOUNG LEE

Department of Meteorology, The Pennsylvania State University, University Park, Pennsylvania

(Manuscript received 14 June 1996, in final form 28 October 1996)

ABSTRACT

This article describes the generation and maintenance of persistent zonal jets in a two-layer quasigeostrophic, β-plane channel model, focusing on the transition from a one to a two jet state. For weak and moderate values of surface friction and supercriticality, the transition occurs abruptly as the width of the baroclinically unstable region of the initial flow is gradually increased. Across the transition point, the persistent two jet state is characterized by a smaller value of eddy energy than that for the one jet state. This reduction in eddy energy is due to increased barotropic energy conversion from the eddies to the zonal mean flow. Consistent with this result, the abrupt emergence of two persistent jets is accompanied by sharply defined eddy momentum flux divergence maxima at the critical latitudes between the two jet maxima. Essentially the same behavior is found in the transition from two to three, and three to four jets.

When two or more jets are present, baroclinically growing waves are found to exist along inter-jet *minima*, which are referred to as ''inter-jet disturbances.'' More importantly, the momentum fluxes of the interjet disturbances diverge at the interjet minimum, further decelerating the jets. Unstable normal modes similar to the inter-jet disturbances are also found. It is argued that the systematic wave absorption at the critical latitudes and the momentum flux divergence by the interjet disturbances may play a central role in the persistence of the multiple jets.

1. Introduction

From theoretical (Rhines 1975) and numerical (Williams 1978) studies, it is well known that in the presence of the meridional planetary vorticity gradient β, an upscale energy cascade generates zonal jets in two-dimensional turbulence. Numerical simulations of quasigeostrophic (QG) turbulence show that if the width of the baroclinically unstable region of the initial flow is greater than the inverse of Rhines's cascade-arrest scale, $(\beta/2u_{\rm rms})^{1/2}$, multiple zonal jets can emerge (Williams 1979, 1988) and persist for a remarkably long time (Panetta 1993). Because Panetta (1993) used a model that includes a full zonal and meridional spectrum, this tremendous persistence of the multiple zonal jets seems robust and not an artifact of the model resolution. Such persistent zonal jets can be relevant for several geophysical fluids, including the giant planetary atmospheres (Williams 1978, 1979) and the ocean (Treguier and Panetta 1994).

While the dynamics of multiple zonal jets is of great interest, many of the fundamental properties of the multiple zonal jets are not well understood. For example, why do the multiple zonal jets found by Panetta (1993) persist with no sign of termination? Is the dynamics of each jet within a multiple jet flow different from that of a flow with a single jet? How would the eddy energy and eddy fluxes, whose parameterization has been a long-standing challenge, behave in inhomogeneous turbulence with such zonal jets?

In addressing the questions raised above, this paper describes some aspects of eddy fluxes and eddy energy that are associated with multiple zonal jets, focusing on the transition from a single jet to a double jet state. This paper is organized as follows. Section 2 briefly describes the model, and section 3 presents an overview of the results. Sections 4 and 5 describe the role of critical latitudes and unstable normal modes in the organization and maintenance of the multiple jets. The concluding remarks follow in section 6.

2. The two-layer quasigeostrophic model

The dimensionless equations for the two-layer QG model on a β-plane are

$$\frac{\partial Q_j}{\partial t} + J(\psi_j, Q_j) = -(-1)^j \kappa_T \left(\frac{\psi_1 - \psi_2}{2} - \tau_e \right) - \delta_{j2} \kappa_M \nabla^2 \psi_2 - \nu \nabla^6 \psi_j, \quad (1)$$

where

$$Q_j = \beta y + \nabla^2 \psi_j + (-1)^j \left(\frac{\psi_1 - \psi_2}{2} \right), \qquad j = 1, 2,$$

Corresponding author address: Dr. Sukyoung Lee, Department of Meteorology, The Pennsylvania State University, 503 Walker Bldg., University Park, PA 16802.
E-mail: sl@essc.psu.edu

and $j = 1$ and 2 refer to the upper and lower layers, respectively. The wind field is determined by the relation $(u_j, v_j) = (-\partial\psi_j/\partial y, \partial\psi_j/\partial x)$. The horizontal length scale is the radius of deformation, λ. Time is nondimensionalized by λ/U_0, where U_0 is the horizontal velocity scale. The Ekman damping coefficient κ_M is included in the lower layer only, and δ_{j2} represents the Kronecker delta. The additional parameters are κ_T (strength of radiative damping), ν (biharmonic diffusivity), and β (gradient of the Coriolis parameter). The values of κ_T and ν are fixed at 30^{-1} and 6×10^{-3}, respectively. A complete description of the model appears in Lee and Held (1991).

We use the following form for the initial zonal-mean zonal wind profile to balance the ''radiative equilibrium temperature'' field $\tau_e(y)$:

$$U_e = -2\partial\tau_e/\partial y = \begin{cases} 1 & |y - W/2| < W_c \\ \exp[-(y - W/2)^2/\sigma^2] & |y - W/2| > W_c. \end{cases} \quad (2)$$

This radiative equilibrium zonal wind field is constant in the center of the domain, and exponentially decays to zero outside of this central region. The initial upper and lower layer zonal mean zonal winds are set equal to U_e and zero, respectively (for example, see side panels in Figs. 1a and 1b). The same zonal wind profile was used by Panetta and Held (1988) and Lee and Feldstein (1996). The value of σ is fixed at 4, but W_c is varied. The parameter $2W_c$ measures the meridional width of the baroclinically unstable region of the initial flow.

The model uses finite differencing in the meridional direction and spectral transforms in the zonal direction. The channel width W is fixed at 90, where the walls are located at $y = 0$ and $y = W$. There are 300 grid points between the channel walls. The fundamental zonal wavenumber is 0.1, and there are 20 zonal waves in this model.

There are five sets of experiments; for each set, the values of β and κ_M are fixed, but the value of W_c is varied. One of the experimental sets represents a control, and the remaining four sets are designed to address the sensitivity of the results to the values of β and κ_M. Table 1 summarizes the five experimental sets and provides a title for each set and a range of values for W_c. Results from 60 different runs are presented, and each run is integrated for 2000 model days (λ/U_0) or more to ensure that a statistically steady state is obtained.

In this paper, the eddy energy ϵ (the sum of eddy kinetic and eddy available potential energy) is defined as the eddy energy averaged over the entire channel length in the zonal direction, but only over the ''flat-top'' region of width $2W_c$ in the meridional direction and over both layers. The precise definition of the eddy energy can be found in (3) and (4) below. Various terms in the energy budget, such as the baroclinic and barotropic eddy energy conversions, are also averaged in the same manner.[1]

3. An overview

This section outlines the results from the five sets of experiments. We first describe results from the control run. Figures 1a and 1b show time–latitude segments of the vertically averaged zonal mean zonal winds for a disorganized, one-jet state and a well-organized, two-jet state, respectively. The value of W_c is 10 for the former case and 11 for the latter case. Comparing these two cases, it is clear that the two jets in the $W_c = 11$ case are remarkably persistent. This comparison also illustrates how dramatically the jet structure can change as W_c is varied by a small amount. This type of persistent, well-organized multiple jet is described in great detail by Panetta (1993), using a doubly periodic two-layer QG model.

Figures 2a and 2b show the meridional structure of the first empirical orthogonal function (EOF1, hereafter) of the zonal wind for $W_c = 10$ and $W_c = 11$ of the control experiment, respectively, along with the time-mean zonal-mean zonal winds. In both cases, the structure of EOF1 indicates that the dominant zonal jet variability is characterized by meridional displacement centered around the position of the time-mean jet, but the meridional displacement is more pronounced for $W_c = 10$, consistent with the time–latitude diagram (Fig. 1a). The mechanism for these meridional jet displacements is described in Lee and Feldstein (1996). For $W_c = 11$, the structure of EOF1 represents not only meridional displacements, but also a pulsation of the zonal wind at the channel center; when the two jets move toward (away from) each other, the strength of the interjet minimum at the channel center increases (decreases).

In every experimental set, the transition from one to two persistent jets does not occur abruptly at a precise value of W_c. Instead, there are ranges of values of W_c over which one and two jet states alternate in time. For example, such alternating flows are found for $W_c = 10.5$ in the control experiment. However, for a smaller value of κ_M (WD) or a larger value of β (HB), this transition occurs over a smaller range of values of W_c. Therefore, although the transition does not occur at a single value of W_c, we

[1] The bulk of the eddy energy is confined within the flat-top region. Given that the channel width is fixed, if the eddy energy is averaged over the entire channel, rather than over the flat-top region, the value of ϵ becomes deceptively large as the value of W_c increases. In general, when evaluating the energetics over a confined region, caution is necessary in interpreting the results. However, in this study, the energetics is greatly simplified because the energy fluxes at $y = \pm W_c$ are two or three orders of magnitude less than the baroclinic energy conversion term. Although not described in this paper, additional tests are performed by calculating each term in the energy budget integrated over the entire domain normalized by the zonal available potential energy integrated over the entire domain. In these calculations, the decrease in the normalized eddy energy across the transition point remains robust.

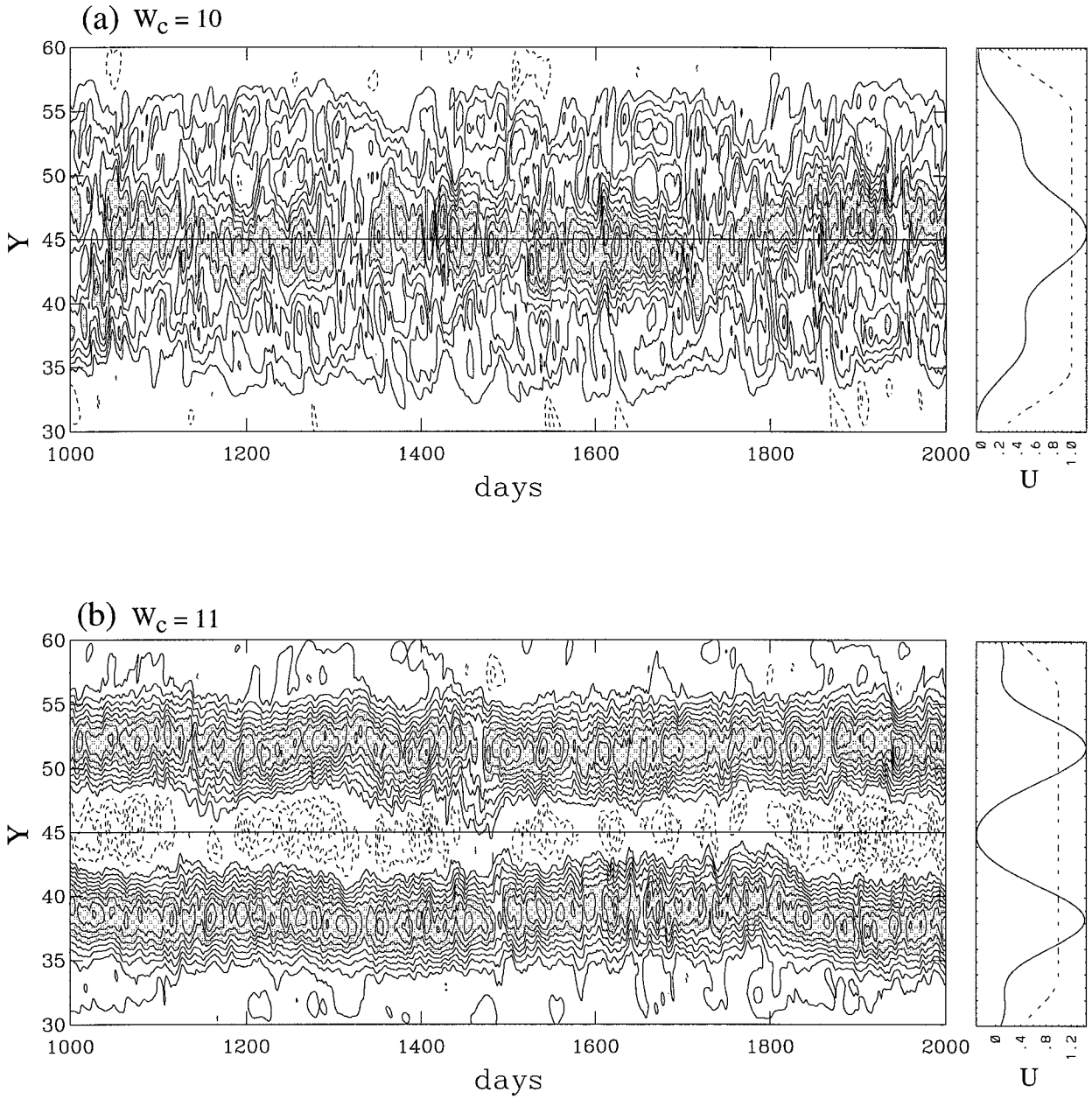

FIG. 1. Latitude–time segment of vertically averaged zonal wind for two jet width (a) $W_c = 10$ and (b) $W_c = 11$, for the control experiment. Solid contours are positive, dashed contours are negative, and the zero contour is omitted. Contour interval is 0.2. Shading denotes values greater than or equal to 1. Corresponding side panels show time-mean vertically averaged zonal wind (solid line) and U_e (dashed line).

TABLE 1. Summary of the parameters used in the five experimental sets. Note that in the text, each experiment is referred to by the abbreviation indicated in the brackets.

Experiment set	β	κ_M	Range of W_c
Control	0.25	0.1	8–28
High beta (HB)	0.35	0.1	7–18
Low beta (LB)	0.15	0.1	7–18
Strong drag (SD)	0.25	0.3	6–12
Weak drag (WD)	0.25	0.04	10–17

refer to the values of W_c over which the transition occurs as the "transition point." Also, the values of W_c larger (smaller) than the transition point are referred to as above (below) the transition point. For example, in the control experiment, $W_c = 10$ is below the transition point, while $W_c = 11$ is above the transition point.

When the transition from one to two jets takes place, ϵ decreases (see Fig. 3a), reversing the tendency of an increase in ϵ with an increase in W_c. For example, the value of ϵ for $W_c = 11$ is *smaller* than that for $W_c = 10$. As W_c is further increased toward $W_c = 19$, ϵ also

increases and a two jet state is maintained. At $W_c = 20$, a three-jet state is established and the value of ϵ drops once again. Similar behavior is found when a four-jet state is established at $W_c = 28$.

From an energetic viewpoint, there are two possibilities that can explain the reduction in ϵ whenever the transition point is crossed and a new well-organized, persistent jet emerges. Consider the eddy energy equation obtained by multiplying ψ_i with the eddy potential vorticity equation of layer i. Adding the two resulting equations, neglecting the biharmonic diffusion terms, and then integrating over the entire domain, yields

$$\frac{\partial}{\partial t}\int_0^W \Bigg[\underbrace{\overline{(u_1'^2 + v_1'^2)}/2 + \overline{(u_2'^2 + v_2'^2)}/2}_{\text{EKE}} + \underbrace{\left(\frac{\overline{\psi_1' - \psi_2'}}{2}\right)^2}_{\text{EAPE}}\Bigg] dy$$

$$= \int_0^W \Bigg[\underbrace{(\overline{U_1} - \overline{U_2})\frac{\overline{(\psi_1' v_2')}}{2}}_{C_{\text{BC}}} + \underbrace{\overline{U_1}\frac{\partial}{\partial y}\overline{(u_1' v_1')} + \overline{U_2}\frac{\partial}{\partial y}\overline{(u_2' v_2')}}_{C_{\text{BT}}}\Bigg] dy$$

$$- \int_0^W \frac{\kappa_I}{2}\overline{(\psi_1' - \psi_2')^2}\, dy - \int_0^W \kappa_M \overline{(u_2'^2 + v_2'^2)}\, dy, \tag{3}$$

where EKE, EAPE, C_{BC}, and C_{BT} denote the eddy kinetic energy, eddy available potential energy, baroclinic energy conversions, and barotropic energy conversions, respectively. The overbar represents the zonal mean. Because the left-hand side of (3) must vanish for a sufficiently long time average, there must be a balance between C_{BC}, C_{BT}, and the various energy dissipation terms. One could use this balance requirement to understand the above decline in ϵ if there was a mathematical relationship between ϵ and one of the energy conversion or dissipation terms. Such a precise mathematical expression exists only if linear potential vorticity damping is used with identical dissipation timescales in both layers. Obviously this is not the case in the present model. Nevertheless, we can obtain insight into this problem by noting in (3) that the thermal (Ekman) damping is linearly proportional to the EAPE (lower layer EKE). Assuming that the upper layer EKE is positively correlated both with the lower layer EKE and the EAPE, one can establish a qualitative relationship,

$$\epsilon \equiv (\text{EAPE} + \text{EKE}) \propto \tau_L(C_{\text{BC}} + C_{\text{BT}}), \tag{4}$$

where τ_L is some linear damping timescale. Although unrealistic, if as discussed above, potential vorticity damping is used, (4) is exact with $\tau_L/2$ being the potential vorticity damping timescale. Therefore, within each set of experiments, where the values of the damping coefficients are held fixed, one can conclude that the decline of ϵ is due to either a decrease in (C_{BC}) or an increase in ($-C_{\text{BT}}$) or their combination.

One sees that C_{BC} essentially increases at a uniform rate from $W_c = 8$ to 28, including through the transition point. However, the barotropic conversion $-C_{\text{BT}}$ increases nearly 30%–40% during the transition, reversing the trend that $-C_{\text{BT}}$ decreases as W_c increases, away from the transition points. Although it is rather difficult to see in Fig. 3a, energy dissipation due to both the thermal and Ekman damping decreases slightly across the transition points, resembling the trend of ϵ. The similarity in the trend between ϵ and energy dissipation due to the thermal and Ekman damping is more ubiquitous in other sets of experiments, shown in Figs. 3b–d, adding confidence in the assumption that led to (4).

The energy budgets for the HB, LB, WD, and SD experiments are shown in Figs. 3b, 3c, 3d, and 3e, respectively. Having demonstrated the robustness of the behavior of ϵ during each of the transitions in Fig. 3a, the values of W_c in these additional experiments are varied only to the extent that transitions from one to two jets are captured except for the HB experiment.

The decline of ϵ associated with the transition is evident in HB and WD, but not the SD and LB experiments. In the HB and WD experiments, the decline in ϵ is due to the increase in $-C_{\text{BT}}$. In the SD case, although $-C_{\text{BT}}$ slightly increases across the transition point, which lies between $W_c = 8$ and 9, ϵ does not decrease because the increase of C_{BC} is larger than that of $-C_{\text{BT}}$. This is consistent with the fact that the meridional shear of the jets is weaker for the SD and LB cases than the other cases, because $-C_{\text{BT}}$ is proportional to the jet shear. Also, if drag is strong enough, the role of $-C_{\text{BT}}$ in the eddy energy balance is expected to become smaller. For the HB experiment, above the transition point C_{BC} increases substantially, generating an even more complex behavior for ϵ. The reason for this large increase of C_{BC} is unclear. As stated above, for the LB experiment, no decline in ϵ is found. In this experiment, although the time-mean jet shows two distinct peaks for $18 \leq W_c$ (Fig. 7b), a persistent

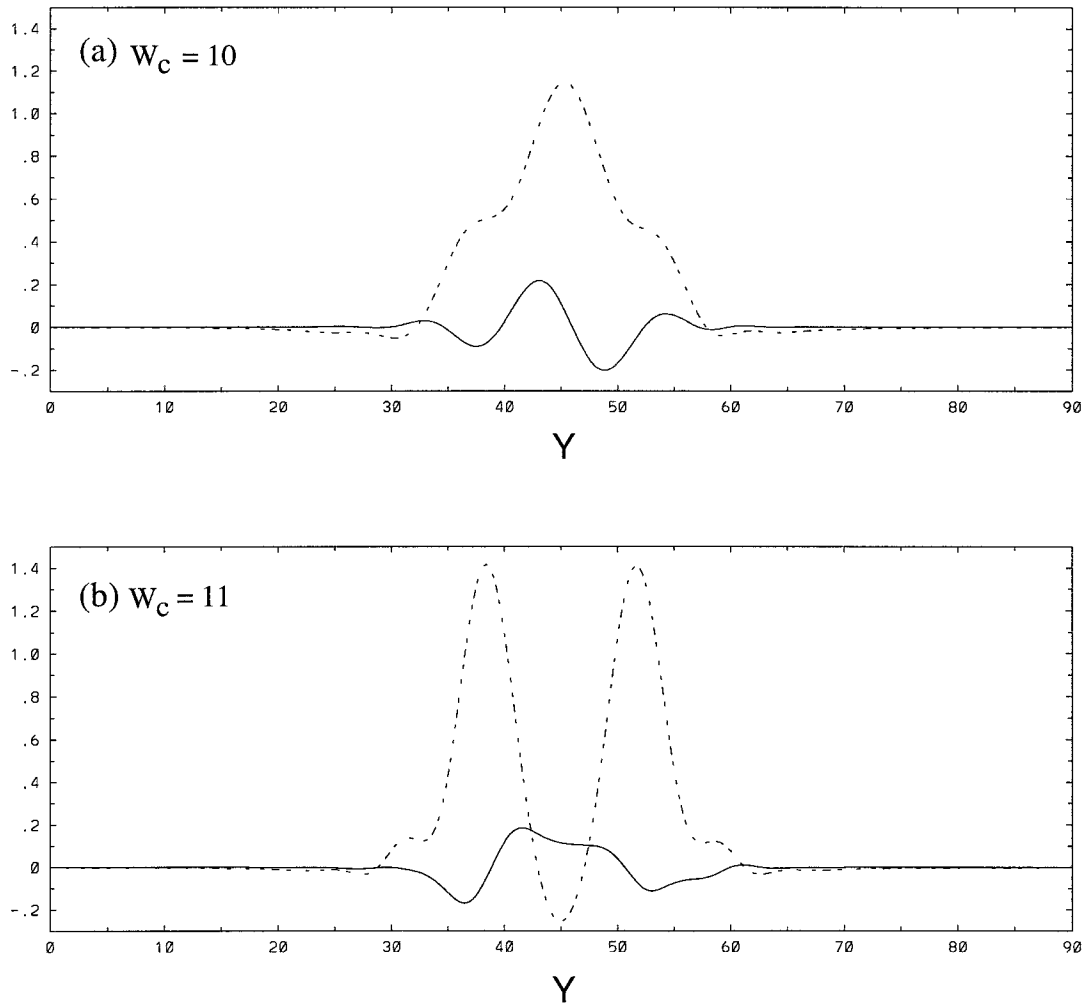

FIG. 2. EOF1 (solid line) and time-mean vertically averaged zonal wind (dashed line) for (a) $W_c = 10$ and (b) $W_c = 11$, for the control experiment.

two jet state was never realized; instead, one and two jet states alternate in an irregular manner. As will be discussed in section 4, we suspect that it is not the mere *occurrence* of two jets but the *persistence* of two jets that is associated with the decline in ϵ.

Lastly, we note that the transition points vary as the values of β and κ_M are changed. For example, the transition point lies between $W_c = 10$ and 11 for the control experiment, whereas it exists between $W_c = 8$ and 9 for the HB experiment. Comparing Figs. 3a–e, it is clear that the value of the transition point is smaller for the HB and SD experiments, relative to that of the control. Not surprisingly, since W_c measures the width of the baroclinically unstable region of the radiative equilibrium flow, just above the transition point, the jet scale in the HB and SD experiments is less than that for the control experiment (see Figs. 5 and 7). Such behavior is consistent with the findings of Panetta (1993), where it was shown that the jet scale in his QG turbulence simulation is well approximated by $L_\beta = 2\pi(u_{\rm rms}/\beta)^{1/2}$; L_β is proportional to the rms eddy velocity $u_{\rm rms}$ and inversely proportional to β. In general, many studies find that the value of $u_{\rm rms}$ decreases as κ_M and β increase. Therefore, as β and κ_M increase, L_β decreases.

4. Role of the critical latitudes in multiple jets

Given the fact that the decline of ϵ associated with the jet transition is robust within a finite region of parameter space, in this section we explore the mechanism behind this behavior in more detail. Ultimately, this should lead to an improved understanding of the abrupt organization of multiple jets and their persistence.

Because the decline of ϵ is due to barotropic energy conversion from the waves to the zonal mean flow, one wonders whether the behavior of ϵ as well as the maintenance of the zonal jets can be understood in terms of wave absorption at critical latitudes, where the zonal-mean zonal wind velocity equals the waves' phase velocity. Baroclinic life-cycle experiments (e.g., Feldstein

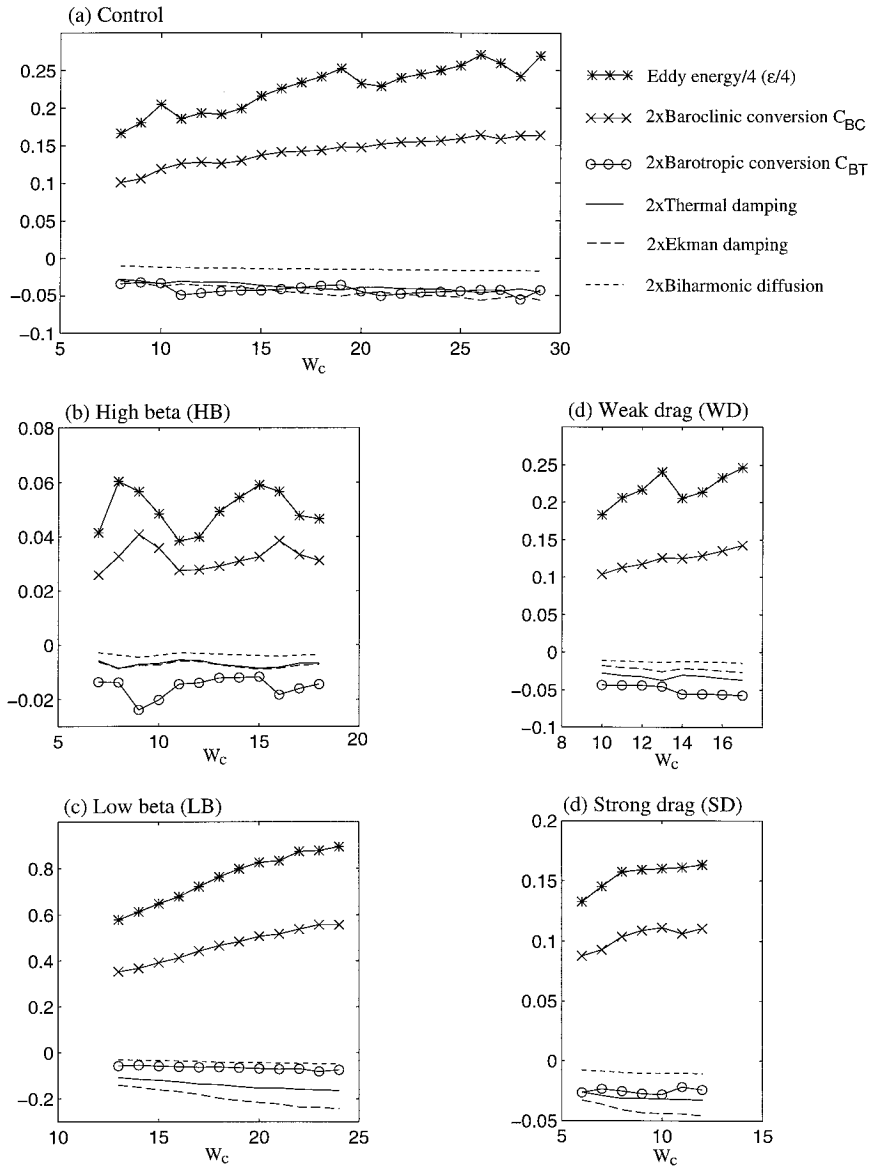

FIG. 3. Eddy energy ϵ, baroclinic energy conversion C_{BC}, barotropic energy conversion C_{BT}, energy dissipation by thermal damping, and Ekman friction as a function of W_c for (a) control, (b) HB, (c) LB, (d) WD, and (e) SD experiments.

and Held 1989) show that the eddy momentum flux divergence occurs near critical latitudes, thus decelerating the zonal mean wind in that region. Although it is yet to be shown, the systematic wave absorption associated with critical latitudes *can* explain the persistence of the multiple jets.

In order to investigate the possible role of the critical latitudes, we use phase speed spectra of the eddy fluxes, as described by Randel and Held (1991). For each latitude, cospectra of zonal mean eddy heat flux and zonal mean eddy momentum flux convergence are calculated as a function of zonal wavenumber and frequency. One can then calculate the sum of the contributions from all zonal wavenumbers and corresponding frequencies toward a specific zonal phase speed. The results of this procedure are presented as contour diagrams of wave covariance versus phase speed and latitude. For conciseness, such diagrams will be referred to as PL (phase velocity–latitude) diagrams throughout this paper.

a. The control case

Figures 4a and 4b show PL diagrams of eddy heat flux and eddy upper-layer vorticity flux, or, equivalently, eddy momentum flux convergence, for the control, $W_c = 10$ case, just below the transition point. In order

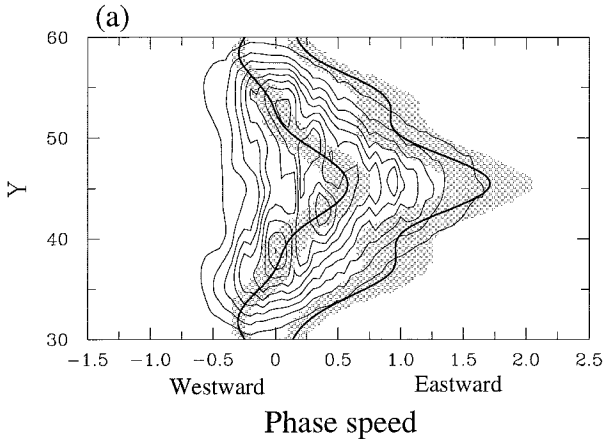

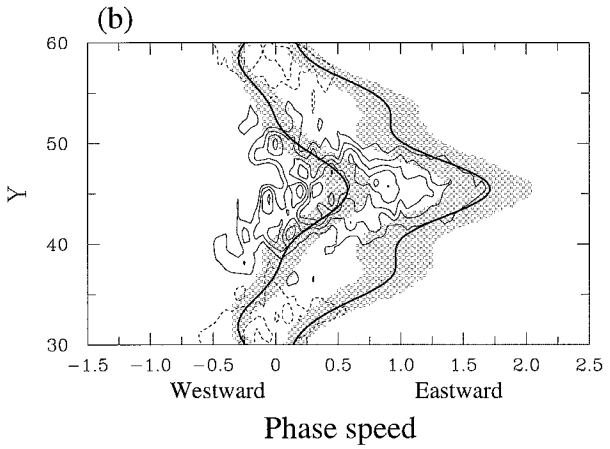

FIG. 4. Contours of (a) eddy heat flux and (b) upper-layer eddy relative vorticity flux versus latitude and phase speed for the control experiment, $W_c = 10$. Contour interval is 0.02. Time-mean zonal-mean zonal winds in both layers are indicated by heavy lines, and shading denotes plus and minus one standard deviation of the zonal winds.

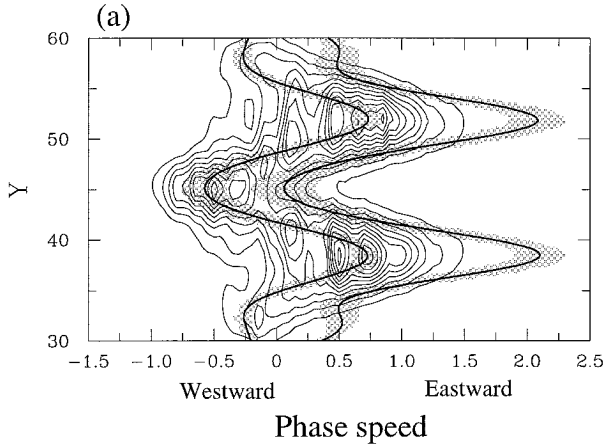

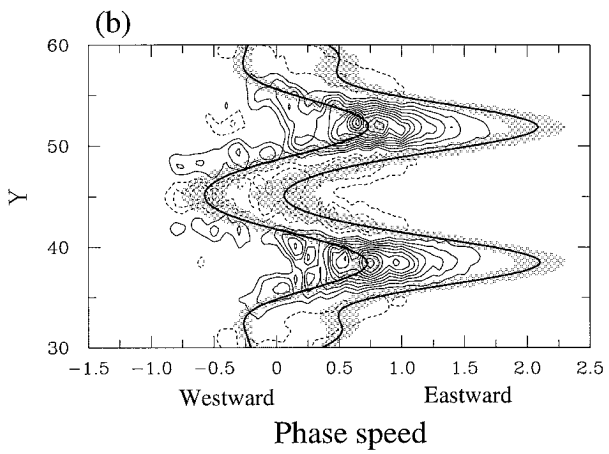

FIG. 5. As in Fig. 4 except for the control experiment $W_c = 11$.

to indicate critical latitudes for a given phase velocity, the time-mean zonal wind speed is superimposed on these PL diagrams. For example, in Fig. 4b, for a phase velocity of 0.75 there are two upper-layer critical latitudes, that is, $y = 35$ and 75, at which the time-mean zonal wind velocity is also 0.75. There is a broad region of eddy heat flux bounded by the upper-layer zonal winds with its maximum at the latitude of the westerly jet maximum. Also, the momentum flux convergence (divergence) maximum exists along the westerly jet maximum (flanks). According to linear critical layer theory, Rossby waves that propagate away from source regions are absorbed at their critical layers, manifesting themselves in a maximum momentum flux divergence in those regions. However, Fig. 4b shows that the momentum flux divergence maxima occur next to, rather than superimposed upon, the critical latitudes. The same behavior was found in idealized baroclinic life-cycle calculations in a two-layer model (Feldstein and Held 1989) and observations (Randel and Held 1991).

Figures 5a and 5b, respectively, show PL diagrams for eddy heat and upper-layer eddy vorticity flux for the control, $W_c = 11$ case, where two persistent jets coexist. There are two eddy heat flux maxima at $y = 38$ and 52, each associated with a westerly jet maximum. At the outer wings of the two jets (i.e., $y < 38$ and $y > 52$), the eddy momentum flux divergence maxima occur close to the critical latitudes. Between the two jet maxima ($38 < y < 52$), the momentum flux divergence maximum coincides with the time-mean zonal wind remarkably well. Along these inner flanks of the jets, for a given phase speed, the momentum flux divergence is confined in a narrow zone of latitudes centered around the critical latitude. As will be discussed later, we suspect that these well-defined latitudes of wave absorption are largely responsible for the abrupt organization of the two persistent jets.

In Figs. 4 and 5, the shading denotes plus and minus one standard deviation of the zonal winds. Perhaps, due to this well-organized region of wave absorption, fluc-

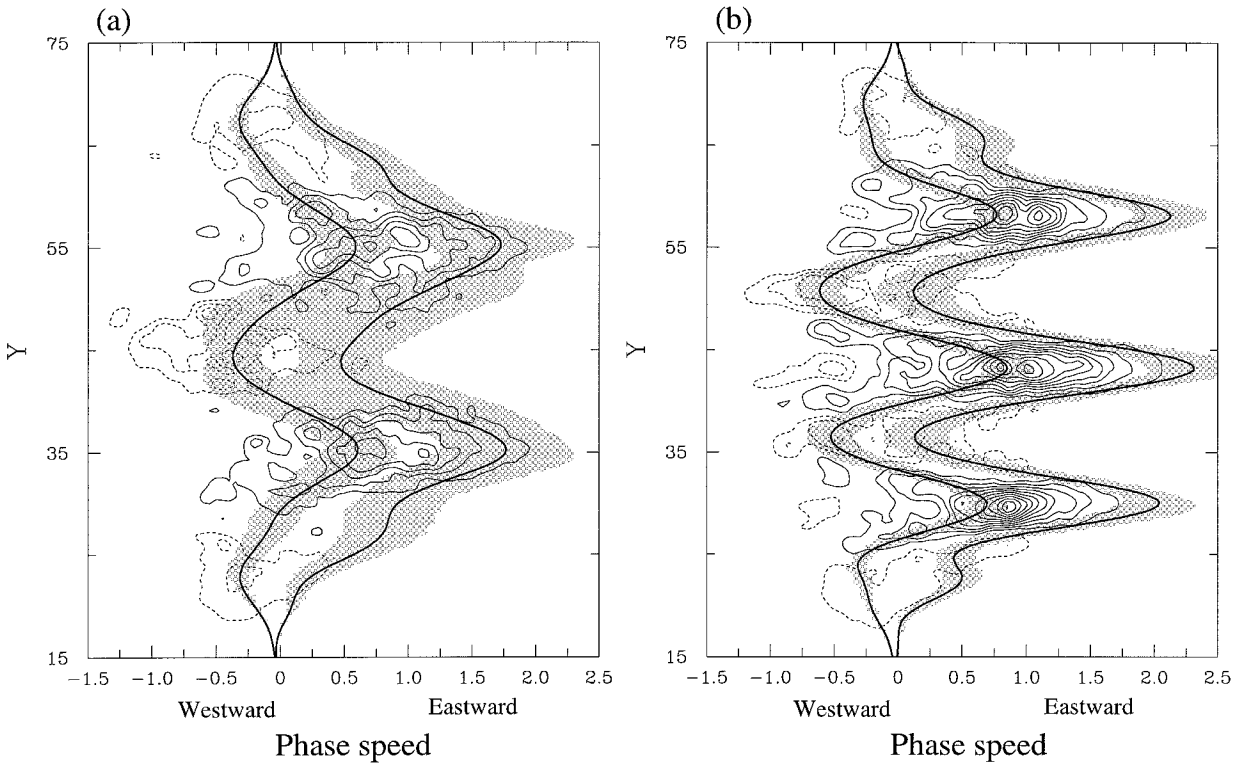

FIG. 6. Contours of upper-layer eddy relative vorticity flux versus latitude and phase speed for the control experiment, (a) $W_c = 19$ and (b) $W_c = 20$. Contour interval is 0.02. Time-mean zonal-mean zonal winds in both layers are indicated by heavy lines, and shading denotes plus and minus one standard deviation of the zonal winds.

tuation of the zonal winds about their mean position is notably smaller for $W_c = 11$ than for $W_c = 10$.

In the $W_c = 11$ case, intriguing behavior is found at the inter-jet minimum ($y = 45$), where a momentum flux divergence maximum exists at phase speeds centered around -0.5. Clearly, this cannot be explained by wave breaking associated with upper-layer critical latitudes. The momentum flux divergence at the inter-jet minimum, by decelerating the zonal winds locally, must also play a role in isolating the two jets from each other. This momentum flux divergence is accompanied by a local heat flux maximum (see Fig. 5a) at precisely the same location. In this paper, these waves near the inter-jet minimum are referred to as ''inter-jet disturbances.'' The spatial relationship between the eddy momentum and heat fluxes of the inter-jet disturbances is distinctly different from those associated with the much more familiar westerly jets, described above. Also, note that this jet inter-jet minimum is different from an easterly jet (Kwon 1989; Feldstein 1991, among others) in one basic aspect: the vertical shear is positive rather than negative. To our knowledge, this well-defined baroclinic wave located at the inter-jet minimum, which exhibits the eddy flux features described above, has not been reported in the literature. Its potential importance for isolating the two jets warrants further investigation, and such attempts are made by analyzing the linear stability of the time-mean flow. The results are presented in section 5.

Two notable features, namely, 1) the coincidence of the critical latitudes and the latitudes of maximum momentum flux divergence, and 2) the prominence of the inter-jet disturbances, are once again observed when three jets emerge from two jets. Figures 6a and 6b show the PL diagrams for the upper-level momentum flux convergence for the $W_c = 19$ and 20 cases, respectively. For $W_c = 20$, just above the transition point from two to three jets, well-defined momentum flux divergence maxima exist at the critical latitudes (Fig. 6b). In addition, the inter-jet disturbances are also prominent at the latitudes of the two interjet minima. In contrast, for $W_c = 19$ (see Fig. 6a), the momentum flux divergence is visible in the vicinity of the interjet minimum and on the outer flanks of the two jets. Although the meridional jet displacement is greater for $W_c = 19$ than for $W_c = 11$ and 20 (compare the shaded areas in Figs. 5b, 6a, and 6b), the two jets are well separated at all times (not shown). Such behavior suggests that the interjet disturbances alone are able to isolate jets from each other.

b. Sensitivity experiments

Figures 7a–d show the PL diagrams of the upper-layer eddy vorticity flux for selected runs, from the HB,

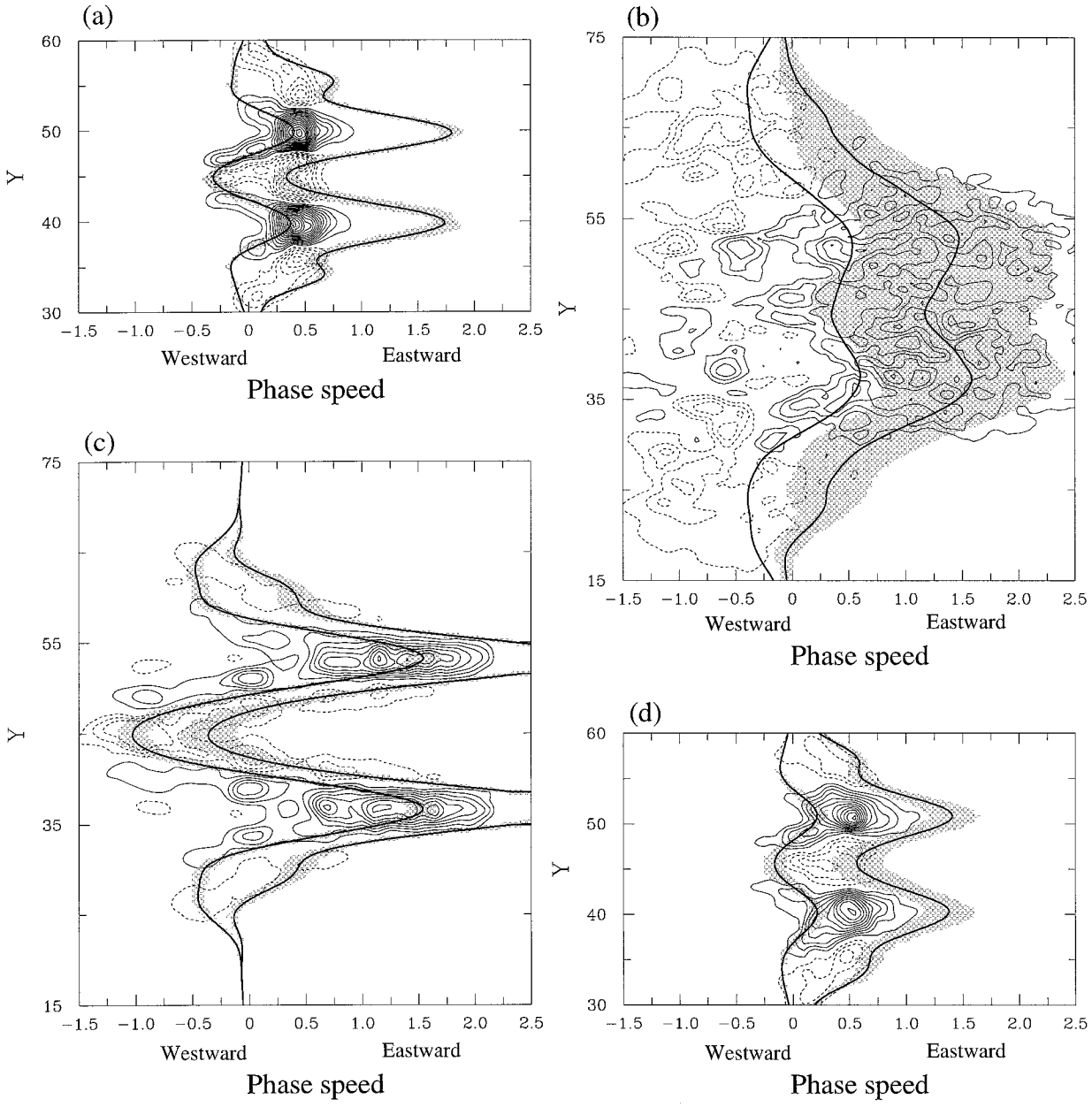

FIG. 7. As in Fig. 6 except for the following experiments: (a) HB, $W_c = 10$; (b) LB, $W_c = 18$; (c) WD, $W_c = 14$; and (d) SD, $W_c = 9$. (e) Eddy heat flux vs latitude and phase speed for the WD, $W_c = 14$ experiment. Contour interval is 0.01 for (a) and 0.02 for (b)–(e).

LB, WD, and SD experiments. Except for the LB case, these runs correspond to the two-jet state cases just above the transition point.

For the HB case (Fig. 7a), the transition point from one to two jets lies from $9 < W_c < 10$, for somewhat smaller W_c than that for the control case as noted earlier (see Fig. 3b). Above the transition point, that is, $W_c = 10$, well-defined regions of eddy momentum flux divergence are seen on both sides of the two jets.

For the LB case (Fig. 7b), as noted earlier, the transition point is no longer well defined. At this parameter setting, one and two jet states alternate in an irregular manner over a wide range of W_c. As the value of W_c is increased gradually, the flow falls into the two jet state more frequently, but the two jets are not maintained persistently, unlike the other cases.

Comparing the HB, control, and LB cases, it is clear that both the persistence of the jets and the abruptness of the transition from a single to a double jet state are apparent only for moderate and large values of β. This is consistent with the theory that on a β-plane, once the upscale energy cascade is halted at total wavenumber $(\beta/2u_{\text{rms}})^{1/2}$, the energy is further cascaded into zonal jets (Rhines 1975). Therefore, as the value of β decreases,

one would expect that zonal jets will be less apparent. In contrast to previous QG turbulence calculations (e.g., Rhines 1979), which examine the generation of multiple jets using an initial value approach, the calculations performed in this study emphasize the persistence of the multiple jets in a forced/dissipative flow. Based on the experiments described in this paper, we suggest that in a forced/dissipative QG flow, it is 1) the wave absorption along the upper-layer critical latitudes and 2) the momentum flux divergence by the interjet disturbances that are responsible for the persistence of the zonal jets. To this end, it is worth noting that the shaded area that measures the zonal wind fluctuation (see Figs. 7a–d) is much smaller for the HB and WD cases where the wave absorption along the critical latitudes is prominent.

Consistent with this conjecture, for the LB experiment, the phase speeds of the most energetic waves are smaller than the upper-layer zonal jet minimum (see Fig. 7b). Therefore, between the two jets, critical latitudes are nonexistent for most disturbances, making wave absorption at the critical latitudes, if any, extremely limited in that region. In the LB experiment, the waves' intrinsic phase speeds are small because of the relatively large horizontal scale of the waves. (For example, for the control experiment, the wave energy peaks at $k = 5$, while the LB experiment shows a much broader energy spectrum with a peak at $k = 3$.) The above argument can be elaborated as follows. If one takes L_β as the dominant horizontal scale of the waves, then the phase speed of the wave is proportional to $\bar{U} - 2u_{\rm rms}$. Because the supercriticality increases as β decreases, one would expect $u_{\rm rms}$ to increase as β becomes smaller. Therefore, in the presence of the westerly zonal mean wind, that is, for $\bar{U} > 0$, one would expect that the Doppler-shifted phase speed will become smaller as β decreases.

We next describe the effects of surface friction by comparing the WD and SD experiments. As we described earlier, the decline of ϵ across the transition point is sharper as the surface friction is decreased (see Figs. 3d and 3e). Figure 7c indicates that the momentum flux convergence occurs precisely at the critical latitudes, resulting in a stronger meridional shear of the zonal mean zonal flow. With the weak surface friction, the shear remains strong, leading to an enhanced barotropic energy conversion. We also note that in the WD experiment, the eddy heat flux associated with the interjet disturbance is greater than that along the two-jet maxima (see Fig. 7e). Although this point was not explicitly stated, Panetta (1993) also showed a case with weak surface friction where the lower-layer eddy potential vorticity flux, which is dominated by the eddy heat flux, reaches a local maxima at local jet minima (see Fig. 3b of Panetta 1993). The reason for this behavior remains unclear. However, once the interjet disturbance is better understood, we expect that insight into this phenomenon can be obtained.

From the foregoing discussion, one expects that the decrease of ϵ across the transition point must be relatively small, if any, when the surface friction is strong. Consistent with this, the PL diagram of the upper-layer eddy vorticity flux (Fig. 7d) does not show two well-defined regions with negative values between the two-jet maxima, unlike the control and WD cases.

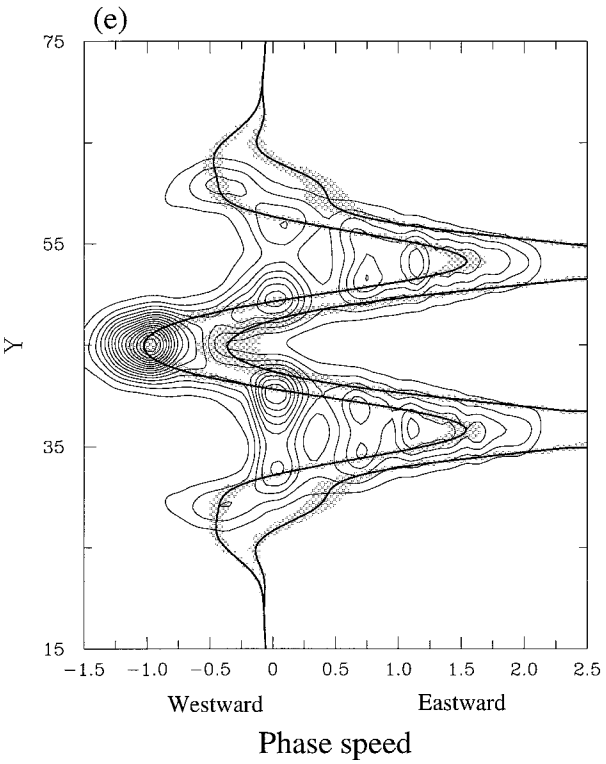

FIG. 7. (*Continued*)

5. Linear stability analysis

Although the relevance of linearly unstable modes to the atmosphere as well as to nonlinear models can be challenged in a number of different ways, in order to understand the interjet disturbances, a natural first step is to study linearly unstable modes. Figures 8a, 8b, 8c, and 8d, respectively, show the meridional structure of the streamfunction amplitude, heat flux, relative vorticity flux, and potential vorticity flux of the fastest growing normal mode of the time-mean flow for the control, $W_c = 11$ case. The growth rate and zonal wavenumber of this fastest growing normal mode are 4.6×10^{-2} and 0.6, respectively. In both layers, the maximum streamfunction amplitude (Fig. 8a) occurs at $y = 45$, the interjet minimum. This mode grows baroclinically, and the heat flux (Fig. 8b) reaches its maximum at the interjet minimum. More importantly, the momentum flux divergence maximum also occurs at the interjet minimum, flanked by momentum flux convergence on either side at $y = 43$ and 47 (see Fig. 8c). Consistent with this heat and relative vorticity flux structure, the potential vorticity flux (Fig. 8d) in either layer peaks at the interjet

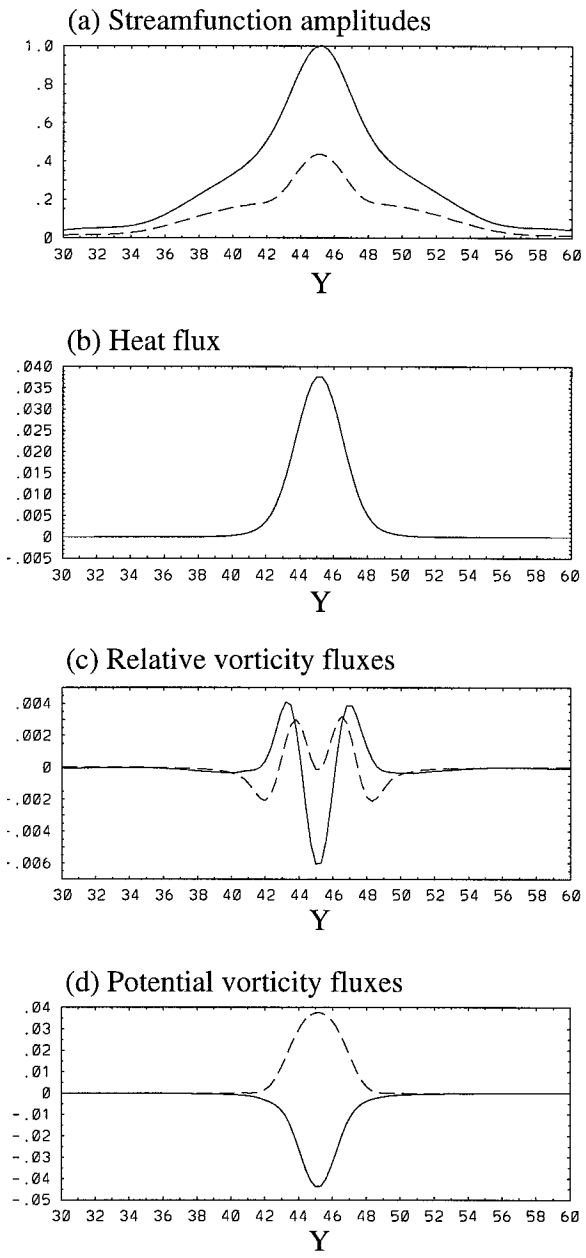

FIG. 8. Meridional structure of the fastest growing normal mode for the control experiment, $W_c = 11$. In (a), (c), and (d) solid (dashed) lines are for the upper (lower) layer. The amplitudes are normalized by the maximum amplitude of the upper-layer streamfunction.

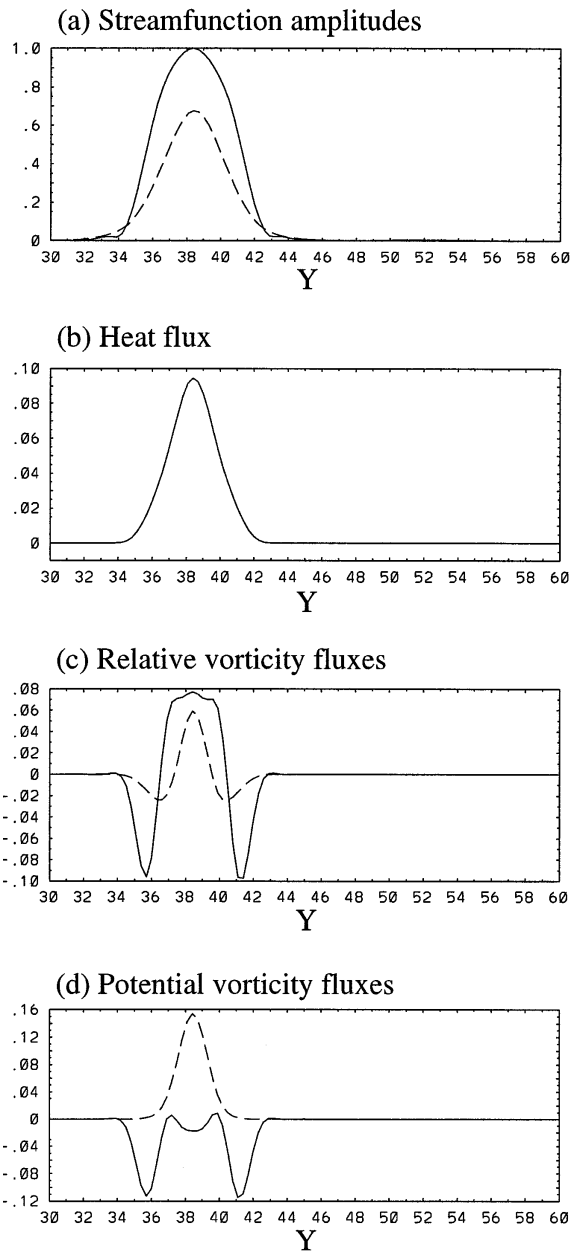

FIG. 9. As in Fig. 8 except for the second fastest growing normal mode for $k = 0.7$ in the control experiment.

minimum. We give the name ''inter-jet mode'' to normal modes with this distinct structure, in contrast to ''conventional'' normal modes that have their maximum heat flux and maximum momentum flux convergence at the jet maximum (see Figs. 9b and 9c).

This inter-jet mode is robust; for the $W_c = 11$ case of the control experiment, given any zonal wavenumber the fastest growing normal mode possesses essentially the same structure as that for $k = 0.6$ (see Fig. 8). The growth rate, phase speed, and structural characteristics of some selected unstable modes, including the fastest growing mode, are summarized in Table 2. For $k \leq 0.4$ and $k \geq 1.0$, there is no unstable mode.

The inter-jet mode is also the most unstable normal mode in each of the four selected runs from the HB, LB, WD, and SD experiments, described in section 4b. Furthermore, except for the LB case, the interjet mode is the fastest growing normal mode for any given zonal wavenumber. In the LB case, for $k = 0.3$, 0.4, and 0.5, none of the unstable modes take the form of the interjet mode. Recalling that two persistent jets are not found

TABLE 2. Summary of the selected unstable normal modes for the time-mean, zonal-mean flow of the control, $W_c = 11$ case. Rank is based on linear growth rate.

Rank of unstable mode	κ	Growth rate	Phase speed	Description
1	0.5	4.06×10^{-2}	-0.432	Inter-jet mode
1	0.6	4.60×10^{-2}	-0.355	Inter-jet mode
1	0.7	3.87×10^{-2}	-0.301	Inter-jet mode
1	0.8	2.45×10^{-2}	-0.256	Inter-jet mode
1	0.9	0.93×10^{-2}	-0.212	Inter-jet mode
2	0.7	0.89×10^{-2}	0.845	Conventional mode
2	0.8	1.34×10^{-2}	0.905	Conventional mode

in the LB experiment, it is interesting to note that in this case the bulk of the wave energy in the nonlinear integration lies at $k = 0.3$, where an unstable interjet mode does not exist.

The structure of the the interjet mode compares very favorably with the interjet disturbances found in the nonlinear control calculation, for which the dominant zonal wavenumber at the interjet minimum is 0.5. As stated above, for $k = 0.5$, the fastest growing normal mode is the inter-jet mode with a phase speed of -0.432 (see Table 2). In Figs. 5a and 5b, along $c = -0.432$, the local heat flux and momentum flux divergence maxima are clearly seen to lie at $y = 45$. Furthermore, in Fig. 5b, the local momentum flux convergence maxima are present at $y = 42$ and 48, very close to those shown in Fig. 8c.

Unstable conventional normal modes, whose structure is similar to the disturbances growing on the jet maxima, are found only for $k = 0.7$ and $k = 0.8$. In both cases, these unstable modes are the second and third fastest growing modes. Figures 9a–d show the meridional structure of the streamfunction amplitude, heat flux, relative vorticity flux, and potential vorticity flux of the second fastest growing normal mode for $k = 0.7$. The largest amplitude of this mode is found at the southern jet maximum. The third fastest growing normal mode shows identical structure, except that its largest amplitude lies at the northern jet maximum (not shown). As noted earlier, the heat flux maximum occurs at the jet maximum; however, unlike the inter-jet mode, the momentum flux divergences are found away from the jet maximum, that is, at $y \approx 36$ and 41. As a result, the upper-layer potential vorticity flux extrema also occur at the same latitudes, on either side of the jet (Fig. 9d). These latitudes where the greatest upper layer potential vorticity flux occur match with the critical latitudes of the nonlinear integration (see Fig. 5b).

6. Concluding remarks

This paper describes some aspects of quasigeostrophic turbulence in a parameter regime where spontaneously generated zonal jets exist. We focus on the transition from a single to a double jet state. When β is greater than a moderate value (≈ 0.2) and surface friction κ_M is not too strong (κ_M less than ≈ 0.3), the transition occurs abruptly as the width of the baroclinically unstable region of the initial flow is systematically increased. Across this transition point, a disorganized single meridionally meandering jet is replaced by two persistent jets that exhibit much less fluctuation. Close to the parameter value at which the transition occurs, the eddy energy ϵ is smaller for the double jet state than for the single jet. Such behavior goes against the general tendency of ϵ to increase away from the transition point. It is found that barotropic energy conversion from the eddies to the jets is responsible for the local minimum in ϵ in the vicinity of the transition point.

We believe that critical layer absorption plays a crucial role in the abrupt formation and maintenance of the multiple zonal jets, at least near the transition point. Just above the transition point where the flow organizes itself into two persistent jets, eddy momentum flux divergence maxima occur *at* all critical latitudes associated with both jets. Such a systematic zonal mean flow deceleration at the critical latitudes, caused by the eddy momentum flux divergence, results in a strong meridional shear of the zonal-mean zonal flow and hence increases the barotropic energy conversion from the eddy to the zonal mean flow. An exception is found in the LB experiment, where the transition from one to two jets no longer occurs abruptly. Instead, the transition is gradual and the temporal flow evolution is complex, being characterized by an alternation between one and two jet states. Spectral analysis indicates that the dominant zonal wavenumber has a negative phase speed. Hence there are no critical latitudes in the upper layer for this zonal wavenumber.

When two or more jets coexist, growing baroclinic waves are found to exist along the inter-jet minimum. These waves, referred to as inter-jet disturbances, possess the property that their momentum flux *divergence* occurs at the same latitude as their heat flux *maximum*. One might expect this result because a positive momentum flux divergence at an inter-jet minimum implies that the inter-jet disturbances are tilted along the shear of the zonal-mean zonal winds. However, this does not have to be the case. In fact, if the potential vorticity gradient of the basic flow changes sign in the vertical, which is indeed the case in our calculations, there is no obvious way to predict the direction of the vertically integrated momentum flux (Held 1975), although some general rules are found for a weakly nonlinear flow (e.g., Held and Andrews 1983). Because the momentum flux divergence decelerates the zonal jet at its local minimum, we suspect that the interjet disturbance plays an important role in maintaining the multiple jets by separating them from each other. In fact, away from the transition point, it appears that the inter-jet disturbance is the main player that decelerates the zonal flow between the two jets (see Fig. 6a). The structure of the heat and momentum fluxes of these inter-jet distur-

bances are remarkably well captured by the fastest growing normal mode. The inter-jet disturbance becomes more prominent as drag is reduced. Given its potential importance for maintaining multiple zonal jets, this inter-jet disturbance warrants further investigation. It is also worth noting that existence of this type of inter-jet disturbance is hinted at in a general circulation model (Williams 1988). In that study, when the rotation rate of the earth is increased by more than a factor of 2, more than two eddy-driven jets emerge. As Williams (1988) points out, the poleward eddy heat flux is continuous with latitude, whereas the eddy momentum flux shows clear convergence (divergence) at the jet maxima (interjet minimum). It would be of interest to construct the PL diagram with such calculations, in order to test the existence of inter-jet disturbances in more realistic models.

From the results of the analyses presented in this paper, it is not completely clear as to how the abrupt splitting of the jet occurs. Given an eddy meridional scale that is solely determined by the internal dynamics of the flow as the width of the baroclinically unstable region gradually increases, there must be some point at which two eddies can simultaneously fit in the meridional direction. When this condition is met, two jets can be spontaneously generated in association with these eddies. However, in forcing these two jets, we speculate that each eddy creates its own ''cavity'' because of the wave absorption at its critical latitudes, further isolating itself from the other eddy. This isolation is enhanced by the formation of the inter-jet disturbances. In this manner, two persistent jets may organize abruptly with only a small increase in the width of the baroclinically unstable region.

Although not presented in the text, the linear stability analysis of the initial flow cannot predict the number of jets in the statistically steady state. In particular, the structure and growth rate of normal modes growing on the initial flow are essentially the same on either side of the transition point. For example, in the control experiment with $W_c = 10$ and $W_c = 11$, the fastest growing normal mode is found at $k = 7$, with the structure of a conventional unstable normal mode.

To the extent that radiative forcing of the atmosphere and the action of the wind stress on the ocean surface are dynamically equivalent, the results of this paper imply the need for additional complexity in eddy flux and energy parameterizations, in particular for noneddy resolving ocean models.

Acknowledgments. This research was supported by the National Science Foundation through Grant ATM-9416701. Comments by Dr. Steven Feldstein, Prof. Peter Bannon, and Prof. John Clark on the early version of this manuscript are greatly appreciated. Thanks are also due to Dr. Gareth Williams for suggesting the use of better terminologies and for pointing out his GCM calculations (Williams 1988) that hint at the existence of the interjet disturbances. Comments by an anonymous reviewer are also appreciated.

REFERENCES

Feldstein, S. B., 1991: A comparison of the westerly nonlinear instability of westerly and easterly jets in a two-layer beta-plane model. *J. Atmos. Sci.,* **48,** 1701–1717.

——, and I. M. Held, 1989: Barotropic decay of baroclinic waves in a two-layer beta-plane model. *J. Atmos. Sci.,* **46,** 3416–3430.

Held, I. M., 1975: Momentum transport by quasi-geostrophic eddies. *J. Atmos. Sci.,* **33,** 1494–1497.

——, and D. G. Andrews, 1983: On the direction of the eddy momentum flux in baroclinic instability. *J. Atmos. Sci.,* **40,** 2220–2231.

Kwon, H. J., 1989: A reexamination of the genesis of African waves. *J. Atmos. Sci.,* **46,** 3621–3631.

Lee, S., and I. M. Held, 1991: Subcritical instability and hysteresis in a two-layer model. *J. Atmos. Sci.,* **48,** 1071–1077.

——, and S. B. Feldstein, 1996: Mechanism of zonal index evolution in a two-layer model. *J. Atmos. Sci.,* **53,** 2232–2246.

Panetta, R. L., 1993: Zonal jets in wide baroclinically unstable regions: Persistence and scale selection. *J. Atmos. Sci.,* **50,** 2073–2106.

——, and I. M. Held, 1988: Baroclinic eddy fluxes in a one-dimensional model of quasigeostrophic turbulence. *J. Atmos. Sci.,* **45,** 3354–3365.

Randel, W. J., and I. M. Held, 1991: Phase speed spectra of transient eddy fluxes and critical layer absorption. *J. Atmos. Sci.,* **48,** 688–697.

Rhines, P. B., 1975: Waves and turbulence on a β-plane. *J. Fluid Mech.,* **69,** 417–443.

——, 1979: Geostrophic turbulence. *Annu. Rev. Fluid Mech.,* **11,** 401–441.

Treguier, A. M., and R. L. Panetta, 1994: Multiple zonal jets in a quasigeostrophic model of the Antarctic circumpolar current. *J. Phys. Oceanogr.,* **24,** 2263–2277.

Williams, G. P., 1978: Planetary circulations: 1. Barotropic representation of Jovian and terrestrial turbulence. *J. Atmos. Sci.,* **35,** 1399–1426.

——, 1979: Planetary circulations: 2. The Jovian quasi-geostrophic regime. *J. Atmos. Sci.,* **36,** 932–968.

——, 1988: The dynamical range of global circulations—I. *Climate Dyn.,* **2,** 205–260.